phys. stat. sol. (c) **1**, No. 6, 1367–1376 (2004) / **DOI** 10.1002/pssc.200304070

Monte Carlo simulation of high-order harmonics generation in bulk semiconductors and submicron structures

D. Persano Adorno[*, 1], **M. Zarcone**[1], **G. Ferrante**[1], **P. Shiktorov**[2], **E. Starikov**[2], **V. Gružinskis**[2], **S. Pérez**[3], **T. González**[3], **L. Reggiani**[4], **L. Varani**[5], and **J. C. Vaissière**[5]

[1] Dipartimento di Fisica e Tecnologie Relative, Universitá di Palermo, Viale delle Scienze, Edificio 18, 90128 Palermo, Italy

[2] Semiconductor Physics Institute, A. Goštauto 11, 2600 Vilnius, Lithuania

[3] Departamento de Física Aplicada, Unversidad de Salamanca, Plaza de la Merced s/n, 37008 Salamanca, Spain

[4] INFM – National Nanotechnology Laboratory, Dipartimento di Ingegneria dell' Innovazione, Università di Lecce, Via Arnesano s/n, 73100 Lecce, Italy

[5] Centre d'Electronique et de Micro-optoélectronique de Montpellier (CNRS UMR 5507), Université Montpellier II, 34095 Montpellier Cedex 5, France

Received 2 October 2003, accepted 4 October 2003
Published online 19 February 2004

PACS 42.65.Ky, 72.20.Ht, 72.30.+q, 72.70.+m

To qualify the feasibility of standard semiconductor materials and Schottky-barrier diodes (SBDs) for THz high-order harmonic generation and extraction, the harmonic intensity, intrinsic noise and signal-to-noise ratio are calculated by the Monte Carlo method when a periodic high-frequency large-amplitude external signal is applied to a semiconductor device. Due to very high signal-to-noise ratio heavily doped GaAs SBDs are found to exhibit conditions for frequency mixing and harmonic extraction that are definitively superior to those of bulk materials.

1 Introduction

Nonlinear processes involving high-order harmonic generation from a bulk semiconductor or semiconductor structure subject to intense radiation field have been widely investigated in recent years. This wide interest has been motivated by the possible applications as frequency converter to the sub- and near-THz region, where other techniques are ineffective or difficult to be applied. Starting from an available source of fundamental signal in the frequency range $f = 100 - 300$ GHz [1], to achieve generation in the THz region one needs: (i) either to perform a multicascade multiplication by using frequency doubling and tripling [1], (ii) or to extract the 5th, or higher order harmonic, of the fundamental signal. For this sake, wide use is made of the nonlinearity of hot-carrier velocity-field (v-E) relation in bulk semiconductors [2-8], or of the nonlinearities of current-voltage (I-U) and capacitance-voltage (C-U) characteristics in Schottky-barrier structures [1,9-12]. These nonlinearities are strongly dependent on the value of the excitation frequency. From one hand, at low frequencies the main features of the high-order harmonic generation follow already from the static v-E, I-U and C-U relations. However, when the frequency of the applied and extracted signals moves towards the THz region, one can expect significant modifications of the mechanisms of harmonic generation (due to the cutoff frequencies of some scattering processes, the onset of new dynamical

* Corresponding author: e-mail: dpersano@unipa.it, Phone: +39 09 166 15 086, Fax: +39 09 166 15 063

effects, etc.). From another hand, the extraction of these harmonics is intrinsically limited by the high-frequency noise characteristics of the nonlinear medium or two-terminal structure. Therefore, the aim of this work is to qualify the feasibility of standard semiconductor materials and/or Schottky-barrier diodes (SBD) to become sources of THz radiation by means of high-order harmonic generation and extraction. To this purpose, the harmonic intensities, the spectral density of current fluctuations and the noise-to-signal ratio are calculated by means of Monte Carlo (MC) simulations when a microwave electric bias is applied to the nonlinear medium or structure.

2 Theoretical background

Our interest is to calculate the intensity of generated harmonics and level of noise, as well as their comparison, under cyclostationary conditions when a large-amplitude microwave electric field $E(t) = E_1 sin(\omega t)$ or voltage $U(t) = U_0 + U_1 sin(\omega t)$ at frequency $\omega = 2\pi f$ is applied to, respectively, a bulk material or a SBD. The main steps of the theory are similar to those described in [8] for the case of bulk materials. Here this approach is generalized to extend the analysis also to the case of semiconductor structures. The main steps are briefly summarized in the following.

The instantaneous value of some physical quantity of interest (carrier velocity in bulk materials, total current flowing across a SBD, etc.),

$$q(t) =< q(t) > +\delta q(t) \tag{1}$$

is subdivided into two parts: (i) a regular one $< q(t) >$, which describes the average response of $q(t)$ to the applied periodic excitation, and, (ii) an irregular part $\delta q(t)$, which describes the instantaneous fluctuations of $q(t)$ with respect to its average value $< q(t) >$.

The regular periodic response of $q(t)$ is obtained by averaging over a large number M of the applied signal periods simulated by the MC method

$$< q(\theta) >= \frac{1}{M} \sum_{l=0}^{M-1} q(t = \theta + lT_\omega), \tag{2}$$

where $T_\omega = 2\pi/\omega = 1/f$ is the applied signal period, and θ the phase time belonging to the interval $0 \leq \theta \leq T_\omega$. Then, the Fourier coefficients of the regular response at the fundamental and high-order harmonics are obtained as:

$$q_m = \frac{1}{T_\omega} \int_0^{T_\omega} < q(\theta) > exp(-im\omega\theta) d\theta, \tag{3}$$

where $m = 0, \pm 1, \pm 2, \pm 3$ is the harmonic order. Within such an approach, the regular response spectrum is characterized by the square modulus of harmonic amplitudes $|q_m|^2$. Note, that by averaging over a sufficiently large number of periods the regular response and its harmonics can be calculated with a rather high accuracy, and any physical noise of the nonlinear structure described by $\delta q(t)$ is excluded from consideration.

The noise analysis is based on MC calculations of the two-time symmetric correlation functions (CF) of the fluctuating part of the response $\delta q(t) = q(t) - < q(t) >$:

$$C_{\delta q \delta q}(\theta, s) =< \delta q(\theta - s/2) \delta q(\theta + s/2) >, \tag{4}$$

which depend on the phase time θ and the correlation time of fluctuations $s = t_1 - t_2$ taken as difference between two time moments t_1 and t_2. As in Eq. (2), here brackets $< ... >$ mean averaging over a large number of simulated periods T_ω. The measurable mean spectral density of fluctuations is then obtained by Fourier transformation of $C_{\delta q \delta q}(\theta, s)$ with respect to s and averaging over θ as:

$$\overline{S}_{\delta q \delta q}(\nu) = \frac{4}{T_\omega} \int_0^{T_\omega} \int_0^{\infty} C_{\delta q \delta q}(\theta, s) cos(2\pi\nu s) ds d\theta. \tag{5}$$

It is evident that such a procedure enables only the fluctuating part of the response to be described.

A direct comparison between the spectra of the regular and noise responses can be carried out by using the finite Fourier transform (FT) of a sufficiently long history $q(t)$. In such a case the spectral density of the total response includes the spectra of both the regular response and noise. For this sake a history of $q(t)$ simulated by the MC method is subdivided into a set of time intervals of duration $T = NT_\omega$, which is usually taken as a large integer number N of the applied signal periods T_ω [8]. Accordingly, the spectral density of the total response becomes:

$$S_{qq}(\nu_n) = 2T < g(\nu_n)g^*(\nu_n) >, \tag{6}$$

where the Fourier coefficients are given by:

$$g(\nu_n) = \frac{1}{T}\int_0^T q(t)exp(-i2\pi\nu_n t)dt. \tag{7}$$

Here $\nu_n = n/T$, with $n = 0,\ 1,\ 2,\ ...$, brackets $< ... >$ denote average over an ensemble of different realizations of $q(t)$ histories during time intervals T. Typically, to perform the finite FT, the simulated history calculated with time step $\Delta t = 1 \sim 10\ fs$ is subdivided into $(10^2 \sim 10^3)$ T-intervals each consisting of about 10^5 points. The advantage of this approach is that both the regular response and noise are simultaneously present in the spectrum of the total response. However, their contributions depend on the sampling time T.

The signal-to-noise ratio is evaluated by supposing the additivity of the regular and noise contributions. Accordingly, the spectral density of the total response can be represented as [8]:

$$S_{qq}(\nu) = \overline{S}_{\delta q \delta q}(\nu) + 2T|q_m|^2\delta_{\nu\nu_m}, \tag{8}$$

where $\nu_m = mf$ and $|q_m|$ are the frequency and amplitude of the m-th harmonic ($m = 1, 2, 3, ...$) of the regular response of $q(t)$ to the applied electric-field or voltage with frequency f, $\overline{S}_{\delta q \delta q}(\nu)$ is the mean spectral density of the fluctuations of the quantity $q(t)$ with respect to its regular time-dependent response $< q(t) >$, $\delta_{\nu\nu_m}$ is the Kroneker symbol, and T is the time interval used to perform the finite FT, which determines the frequency resolution $\Delta\nu = 1/T$ of the spectrum. The explicit presence of T in Eq. (8) means that the regular and the noise contributions can be compared as net powers inside the resolution bandwidth $\Delta\nu$. As shown in Ref. [8], such a representation allows us to express the signal-to-noise ratio in terms of the threshold bandwidth:

$$\Delta\nu_{th} = 2|q_m|^2/\overline{S}_{\delta q \delta q}(\nu_m), \tag{9}$$

in which the net intensity of the intrinsic noise is set equal to the intensity of the m-th harmonic of the regular response, and thus harmonic extraction from the noise level becomes impossible. From Eq. (8) one can also obtain a dimensionless representation of the noise-to-signal ratio as:

$$Q_m \equiv f/\Delta\nu_{th} = \overline{S}_{\delta q \delta q}(\nu_m)f/(2|q_m|^2), \tag{10}$$

which gives the ratio between the noise power and the power of the generated m-th harmonic assuming that the bandwidth used for harmonic extraction takes the maximum possible value $\Delta\nu = f$.

3 Numerical results

To consider the feasibilities provided by bulk semiconductors and advanced nanostructures for THz radiation generation due to high order harmonic extraction we shall compare the characteristics of standard n-type bulk materials, namely: GaAs, InP, InN and GaN at 80 K, and nanometric n^+n-metal GaAs SBD at 300 K subjected to microwave (MW) large-signal excitations.

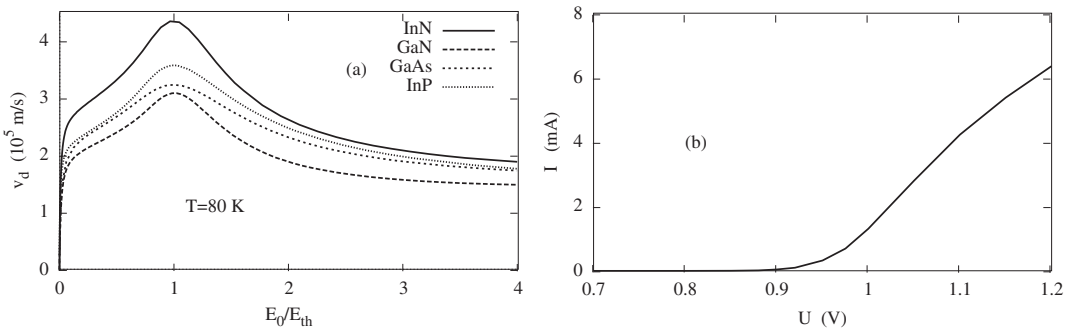

Fig. 1 Static velocity-field and current-voltage relations calculated, respectively, for: (a) bulk semiconductors and (b) nanometric SBD.

Models. Electron scatterings due to ionized impurities, acoustic and polar optical phonons in each valley as well as all intervalley transitions between the equivalent and nonequivalent valleys are accounted for in the usual way [13]. The parameters of the band structure and scattering mechanisms are taken from Ref. [14] (GaAs and InP with impurity concentration $10^{13}\ cm^{-3}$) and from Ref. [15] (InN and GaN with $10^{16}\ cm^{-3}$). Calculations for bulk materials are performed by single-particle MC method by averaging over $5 \sim 10 \times 10^5$ periods of applied MW electric field.

As an example of a nanostructure favorable for THz applications, we have chosen a heavily doped GaAs n^+n-metal SBD with the same parameters of Ref. [11]: n region length $l_n = 0.03$ μm, barrier height $U_b = 1.03$ V, carrier concentrations $n^+ = 8 \times 10^{18}$ cm^{-3} and $n = 1.1 \times 10^{18}$ cm^{-3}, cross-sectional area $A = 7.065 \times 10^{-14}\ m^2$. The n^+ region length l_{n^+} has been reduced to 0.02 μm in order to optimize the computation time without loss of generality. The degeneracy effect is included by determining the final state after scattering with the rejection procedure of Ref. [16]. We focused our interest on the large-signal operation near flat-band conditions, where Schottky diodes typically work. In this regime the tunneling current plays a negligible role as compared to thermionic and displacement currents, and thus it is omitted. Calculations were performed by MC particle (MCP) method coupled with the Poisson equation [17,18]. The self-consistent electric field is updated every 0.2 fs, with a total simulated history duration of about $3 \sim 10$ ns obtained by using $(5 \sim 10) \times 10^3$ particles for the whole SBD.

Static characteristics. Static velocity-field (v-E) and current-voltage (I-U) relations calculated by MC method for the bulk compound semiconductors and the SBD are presented in Fig. 1 (a) and (b), respectively. For bulk materials the average velocity $v_d(E_0/E_{th})$ is shown as function of the static electric field E_0 normalized to the threshold field for Gunn-effect E_{th} equal to 3.25, 9.7, 62 and 132 kV/cm for, respectively, GaAs, InP, InN and GaN. In all cases, the static v-E relation exhibits two main kinks. The first one takes place in the low field region $E_0 \ll E_{th}$ and is due to the onset of an intense polar-optical phonon emission which controls carrier heating in the $\Gamma-$valley and reduces considerably the initial slope of $v_d(E_0/E_{th})$ associated with the low-field mobility. The second kink corresponds to the maximum of the drift velocity and occurs in the intermediate field region centered on the threshold value for Gunn effect, i.e. in concomitance with the appearance of negative differential mobility. To exploit the above properties of the v-E nonlinearity for harmonics generation the large-signal excitation is chosen in the form $E(t) = E_1 sin(2\pi f t)$, with the amplitude value E_1 sufficiently large for the velocity to pass the first and/or the second kinks.

In the case of the SBD, the I-U characteristic exhibits an initial exponential increase in correspondence with an applied voltage U lower than the barrier height $U_b = 1.03$ V (barrier-limited transport regime). For voltages above about $U \approx U_b$ the current increases linearly (flat-band transport-regime) and then tends to saturate due to hot-carrier conditions [11,18]. To exploit in the most effective way the nonlinear region of the I-U characteristic associated with the transition from barrier-limited to flat-band conditions, the

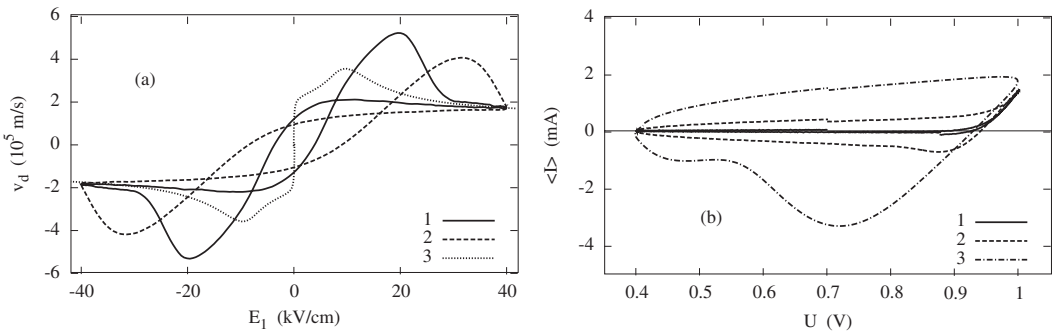

Fig. 2 Dynamic v-E and I-U characteristics calculated, respectively, for: (a) bulk InP and (b) nanometric SBD. Different curves refer to different frequencies (see text).

excitation was taken as $U(t) = U_0 + U_1 sin(2\pi ft)$, with typical values $U_0 = 0.7$ V and $U_1 = 0.3$. In this way the maximum applied voltage is comparable to the barrier height U_b.

Dynamic relations: inertia effects. At sufficiently low frequencies f, dynamical relations are expected to recover those of the static case. However, with the increase of the applied signal frequency the inertia of carrier transport and heating/cooling processes can modify significantly the static v-E and I-U relations, as illustrated in Fig. 2 (a) and (b) for a bulk material or the SBD, respectively. As example of a bulk material, Fig. 2 (a) shows the dynamical total velocity response calculated for InP as a function of the instantaneous value of the MW field $E(t) = E_1 sin(2\pi ft)$ at different frequencies $f = 50$, 200 GHz (curves 1 and 2, respectively) and with the same amplitude of $E_1/E_{th} = 4$. For comparison, curve 3 presents the steady-state $v_d(E_1)$ relation. The effects of the dynamical heating inertia lead to the appearance of a pronounced hysteresis of the dynamical $v_d(E)$ relation.

From one hand, at increasing values of $E(t)$ a velocity overshoot appears caused by the dynamical heating of carriers initially populating the low-energy region of the Γ-valley up to energies sufficient for intervalley transfer and their further quick transition to upper valleys. With frequency increase, this overshoot shifts to a higher field region. From another hand, at decreasing values of $E(t)$ one can detect only the monotonous decrease of the drift velocity without any overshoot or undershoot. This indicates that the electron cooling at decreasing field has a diffusive character in momentum space. Thus, for a sufficiently high amplitude of the alternating field, the stages of carrier heating and cooling are determined by different processes. As a result, the dynamical $v_d(E)$ relation becomes very different from that of the steady-state.

Figure 2 (b) presents the instantaneous total current $< I >$ as a function of the instantaneous periodic voltage $U(t) = U_0 + U_1 sin(2\pi ft)$ applied to the SBD, with $U_0 = 0.7\ V$, $U_1 = 0.3\ V$ and frequencies $f = 0.05,\ 0.5,\ 2$ THz (curves 1 to 3, respectively). As follows from Fig. 2 (b), the inertia of the current response is absent up to $f \approx 0.1\ THz$. Here the $< I(U) >$ diagram follows practically the static I-U relation. At $f > 0.1\ THz$, the instantaneous $< I(U) >$ characteristic begins to differ significantly from that of the static case, what is typical for the strong capacitance-voltage C-U nonlinearity of varactor type [12].

Harmonics generation. The main features of the generated harmonics with the increase of applied signal amplitude are illustrated in Fig. 3 (a) and (b) for bulk materials and SBD, respectively. The modifications of the harmonics with the increase of the applied signal frequency are shown in Fig. 4. In bulk materials, due to the symmetry of the applied signal, only odd harmonics of the fundamental frequency can be excited. As an example, Fig. 3 (a) shows the intensity of 3rd harmonic of the velocity response in bulk materials subjected to a MW electric field of the same frequency $f = 200$ GHz. In all cases there exist two main regions of the applied MW amplitude E_1/E_{th} where the harmonic intensities take maximum values. The first region is a narrow one at amplitudes just below E_{th} (when the nonlinearity is originated by the threshold character of optical phonon emission by electrons in the $\Gamma-$valley). The second region is

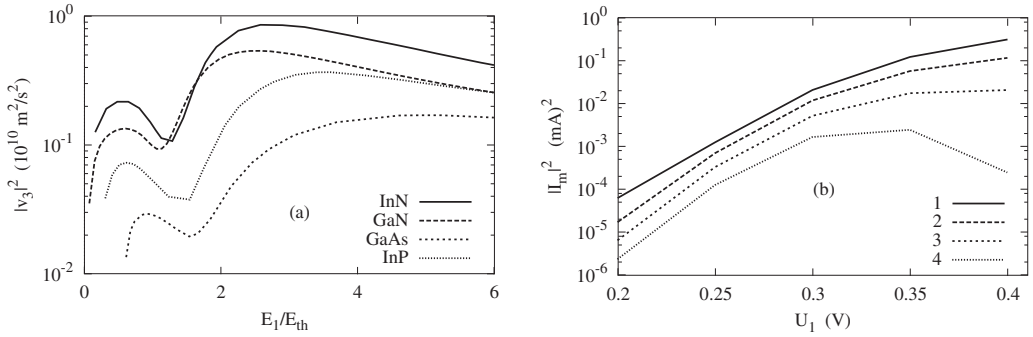

Fig. 3 Harmonic intensity as a function of the applied signal amplitude in: (a) bulk materials and (b) nanometric SBD.

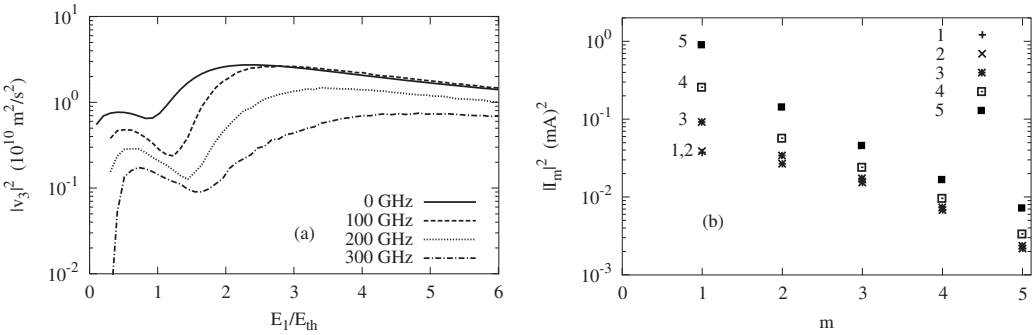

Fig. 4 Harmonic intensity as a function of (a) the applied signal amplitude at different frequencies (third harmonic) in bulk InP, (b) harmonic number m at different frequencies in a nanometric SBD.

a wider one at amplitudes well above E_{th} (when the nonlinearity is caused by intense transfer of electrons into upper valleys). A similar behavior is found also for higher order harmonics.

The influence of the dynamical heating effects on the harmonic generation in bulk materials is illustrated in Fig. 4 (a). Here the intensity of the 3rd harmonic of velocity response, is shown as function of the MW field amplitude calculated by MC method for n-InP at the MW field frequencies $f = 100,\ 200$ and $300\ GHz$. For comparison, the solid lines correspond to the quasi-static approximation when the harmonics intensity is calculated directly from the static v-E relation. As follows from Fig. 4 (a), with the increase of frequency f a general decrease of the intensity of the high order harmonics is observed since, due to the inertia, carrier heating is no longer able to follow the field variation in time. Some increase of the 3rd harmonic intensity at $f = 100\ GHz$ with respect to the quasi-static case is caused by the dynamical overshoot effect discussed above. Nevertheless, at all frequencies the field dependence of the harmonics intensity remains in general the same of that in the quasi-static case, thus confirming the existence of two main regions of harmonic generation related with the low- and high-field kinks of the drift velocity.

In the SBD, due to the presence of the static voltage U_0, both even and odd harmonics can be present. As an example, Fig. 3 (b) reports squared amplitudes of 2nd, 3rd, 4th and 5th harmonics (curves 1 to 4, respectively) generated by the SBD as function of the MW voltage amplitude U_1, with $U_0 = 0.7$ V and $f = 100$ GHz. To somewhat extent, such a behavior is similar to that exhibited by bulk materials in the first nonlinearity region. The hysteresis-like behavior of $< I(U) >$ (see Fig. 2 (b)) is accompanied by a rapid increase with f of the amplitude of both the fundamental and the higher order harmonics, what is typical for the strong C-U nonlinearity of varactor type [12]. This is illustrated by Fig. 4 (b), which shows the squared

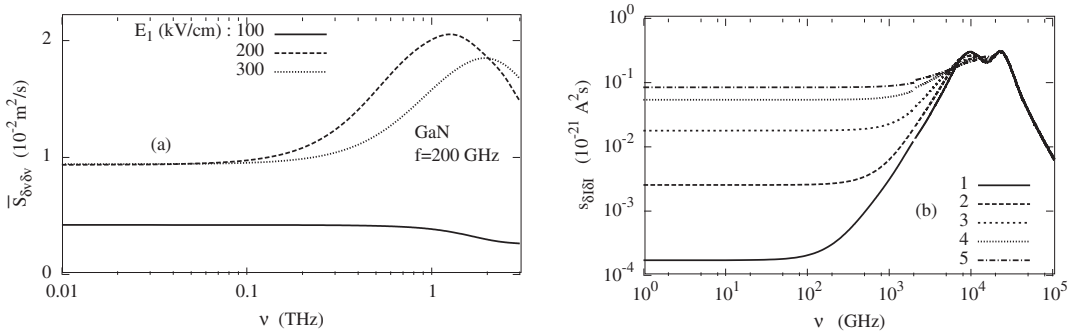

Fig. 5 Spectral densities of intrinsic current noise in: (a) bulk GaN and (b) nanometric SBD.

amplitudes of the first five generated harmonics of the total current density as function of the harmonic order number m calculated for the same conditions of Fig. 3 (b) at frequencies $f = 0.05,\ 0.1,\ 0.5,\ 1,\ 2$ THz (symbols 1 to 5, respectively). For the SBD under test, the C-U nonlinearity dominates over the I-U nonlinearity in the frequency range $0.2 \sim 5$ THz. At a further increase of f, the C-U nonlinearity becomes ineffective, since when approaching the returning carrier resonance [18] the displacement of the depletion region boundary no longer follows the instantaneous value of the applied voltage $U(t)$.

Intrinsic noise. The main features of the intrinsic current noise in bulk materials and SBDs under periodic large-signal operation are illustrated in Fig. 5. As an example of a bulk material, Fig. 5 (a) presents the mean spectral density of velocity fluctuations in GaN at 80 K subjected to a MW electric field of frequency $f = 200$ GHz and different amplitudes E_1 calculated by the correlation function approach. For the lowest fields, just below E_{th}, the spectral density exhibits the usual Lorentzian shape. At increasing fields, above E_{th}, the electron transfer to upper valleys starts playing a dominant role. This leads to a general increase of $\overline{S}_{\delta v \delta v}(\nu)$ in the whole frequency range and to the appearance of a peak due to hot-carriers [19] that takes the maximum value when $E_1 \approx 2E_{th}$. With a further increase of E_1, the value of this peak decreases and shifts to higher frequencies. As follows from Fig. 5 (a) the minimum level of noise is achieved in the first nonlinear region where $E_1 < E_{th}$.

Figure 5 (b) shows the mean spectral density of current fluctuations calculated by the MC method for the SBD at $U_0 = 0.7$ V, $f = 2$ THz and $U_1 = 0.15,\ 0.2,\ 0.25,\ 0.3,\ 0.35\ V$ (curves 1 to 5, respectively). Similar results are obtained at lower frequencies f of the applied signal. The noise spectra exhibit the same features typical of all SBDs under stationary conditions [18], i.e: a low-frequency plateau corresponding to shot noise, a first high-frequency peak related to returning carriers, and a second high-frequency peak due to spontaneous plasma oscillations. As follows from Fig. 5 (b), due to the rather thin depletion region and heavy doping of the SBD considered here, the returning carrier resonance is shifted well above the THz region, so that the noise plateau at low-frequency extends over the THz region. Here, frequency multiplication and mixing can take place at the lowest noise levels for a given U_1. We stress, that the value of the low-frequency noise strongly depends on U_1 and it can increase up to several orders of magnitude with the increase of the applied voltage. Under barrier-limited transport, when $U_0 + U_1 < U_b$, the current noise described above is in good agreement with the universal shot-noise law $S_{\delta I \delta I} = 2q\overline{I}$, and it is related with the concomitant increase of the average current $\overline{I}$ flowing in the SBD. Thus, similarly to the static case, when $U_0 + U_1 < U_b$ the low-frequency noise recovers full shot noise. Moreover, when with a further increase of U_1, so that $U_0 + U_1 \geq U_b$, the I-U moves to flat-band regime, simulations give evidence of some suppression of the shot noise.

Comparison with finite Fourier transform. To ensure that the spectra of generated harmonics and noise are additive and, hence, they can be used to further evaluate the signal-to-noise ratio, it is worthwhile to compare the obtained harmonics and noise intensities with the total response spectra calculated by the finite FT of the fluctuating signal. Such a comparison is illustrated by Fig. 6 (a) and (b) for the cases of bulk InN

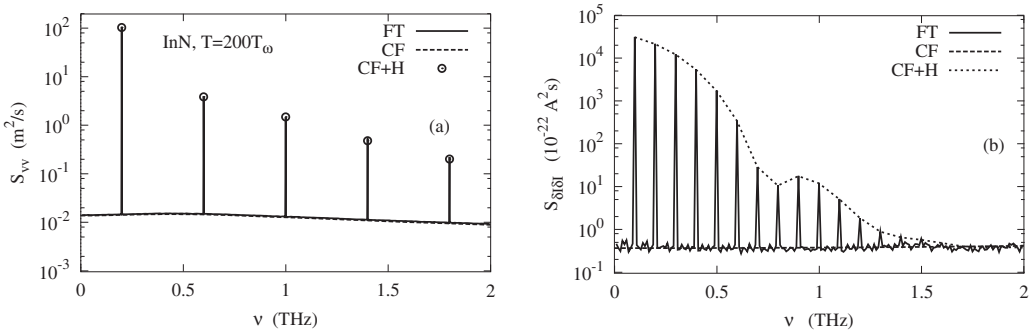

Fig. 6 Finite FT spectra of the total response in: (a) bulk InN and (b) nanometric SBD.

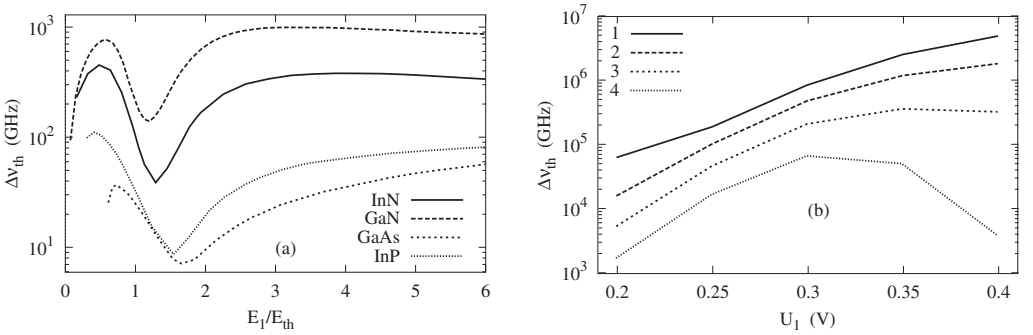

Fig. 7 Threshold bandwidth (signal-to-noise ratio) calculated for: (a) bulk materials and (b) nanometric SBD.

($E_1 = 50$ kV/cm, $f = 200$ GHz) and SBD ($U_0 = 0.7$ V, $U_1 = 0.3$ V, $f = 100$ GHz), respectively. Here, the spectral densities of fluctuations and total response are calculated with three different approaches based on: (i) finite FT of fluctuating velocity and current at time interval $T = NT_\omega$ with $N = 200$ and $N = 10$ for bulk InP and SBD, respectively (FT curves); (ii) CF of velocity and current fluctuations presented by CF curves which practically coincide with the FT-curves outside the spike points; (iii) intensity additivity (IA) where, in accordance with Eq. (8), the spectral density of the total response with the same T as for FT-curves is recalculated by using the intensities of harmonics and the mean spectral densities (CF+H curves). The full coincidence of the CF+H curves with the top of spikes confirms the validity of Eq. (8) and, hence, of Eqs. (9) and (10) in both bulk materials and SBD.

Signal-to-noise ratio. The threshold bandwidth for harmonic extraction $\Delta\nu_{th}$ and noise-to-signal ratio Q_m calculated by Eqs. (9) and (10) by using the intensities of generated harmonics and the mean spectral densities of fluctuations obtained above (see data in Figs. 3 and 5) are shown in Figs. 7 and 8, respectively. As an example for bulk materials, Fig. 7 (a) and Fig. 8 (a) present the threshold bandwidth and noise-to-signal ratios calculated for the 3rd harmonic of the velocity response to a fundamental signal applied to bulk semiconductors at frequency $f = 200$ GHz as function of the normalized field amplitude E_1/E_{th}. The same features calculated for 2nd, 3rd, 4th and 5th harmonics (curves 1 to 4) generated by the SBD at $U_0 = 0.7$ V and $f = 100$ GHz are shown in Figs. 7 (b) and 8 (b) as function of U_1.

In bulk semiconductors, the curves show two main regions of field amplitudes where $\Delta\nu_{th,3}$ is maximum and, correspondingly, Q_3 is minimum, and thus appropriate for harmonic extraction. The first region is a narrow one at amplitudes just below E_{th} where the nonlinearity is originated by the threshold character of optical phonon emission by electrons in the $\Gamma-$valley. The second region is a wider one at amplitudes

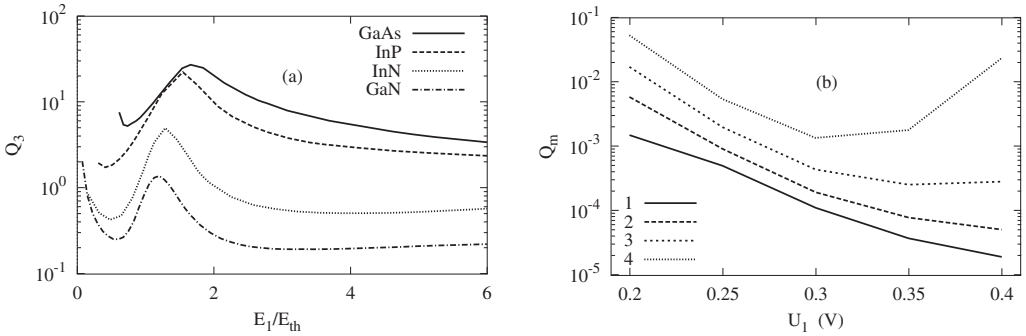

Fig. 8 Noise-to-signal ratio calculated for: (a) bulk materials and (b) nanometric SBD.

well above E_{th} where the nonlinearity is caused by intense transfer of electrons into upper valleys. As follows from Figs. 7 (a) and 8 (a), materials with higher values of E_{th} are characterized by higher threshold bandwidth and, accordingly, lower noise-to-signal ratio value and, thus, they are preferable for the purposes of high-order harmonic extraction. In this respect we notice that, a high value of Q_3 implies that for harmonic extraction from the noise level the resolution bandwidth must be sufficiently narrow. Of course, the increase of the harmonic order leads to an additional deterioration of the harmonic extraction.

When comparing the threshold bandwidth for harmonic extraction and noise-to-signal ratio obtained in SBD (see Figs. 7 (b) and 8 (b)) with that obtained in bulk materials (see Figs. 7 (a) and 8 (a)), we conclude that heavily doped GaAs SBDs exhibit conditions for frequency mixing and harmonic extraction which are definitively superior than those of bulk materials.

4 Conclusions

We have investigated the problem of generating electromagnetic waves in the Tera-Hertz region by using the high-order harmonic technique. As promising candidates for a practical realization we have considered bulk semiconductor materials (nitride in particular) and nanometric GaAs Schottky barrier diodes.

In n-type bulk compound semiconductors generation is found to be primarily related with two main kinks of the static velocity-field characteristic caused by the threshold onset of: (i) spontaneous emission of optical phonons (low-field region), and (ii) carrier transitions between nonequivalent valleys (high-field region). In the low-field region (subthreshold for Gunn effect), the increase of the fundamental signal frequency above 50-100 GHz leads to a systematic decrease of the high-order harmonic intensity generated by the nonlinear medium. In the high-field region (above threshold for Gunn effect) such a reduction can be partially compensated by the additional nonlinearity caused by a pronounced dynamical velocity-overshoot, which in the intermediate frequency region can result even in an increase of the harmonics intensity. However, due to the considerably lower level of the current noise, the low-field region (characterized by a diffusive noise with Lorentzian spectrum) appears to be more favourable for high-order harmonic extraction than the high-field region (characterized by a noise enhancement in the sub-THz region caused by hot-carrier effects).

In Schottky-barrier diodes, the behaviour of the high-order harmonic intensity with the increase of the fundamental frequency is found to be governed by the competitive role played by the I-U and C-U nonlinear characteristics. At relatively small frequencies (sub-TeraHertz region, numerical values depend on material, structure design, doping levels, etc.) harmonics generation is caused mainly by the I-U nonlinearity. Here the harmonic intensity is found to be practically independent of the fundamental signal frequency. With further increase of the fundamental frequency the harmonic intensity starts to increase considerably. Such a behaviour is explained by the growing role played by the dynamical effects induced by the C-U nonlinearity of varactor type, which at sufficiently high frequencies plays a dominant role

in harmonic generation. It is found that: (i) under barrier-limited transport (when the maximum applied voltage $U_0 + U_1 < U_b$), the intrinsic noise is the full shot noise described by the universal $2q\overline{I}$ law; (ii) at $U_0+U_1 \geq U_b$ the intrinsic noise is increasingly suppressed from the full shot noise value. Due to the rather thin depletion region and high doping of the nanometric SBD considered, the returning carrier resonance is shifted well above the THz region, so that the low-frequency noise plateau extends over the THz region. Here frequency multiplication can take place at noise levels equal or below those of full shot noise, thus leading to very high values of the threshold bandwidth (signal-to-noise ratio).

As general conclusion, we found that under nearly similar conditions, nanometric heavily doped GaAs SBDs provide an environment definitively superior to that of bulk semiconductors for extracting high order harmonics above the intrinsic noise level.

Acknowledgements Authors wish to acknowledge the financial support from the french-lithuanian bilateral cooperation n. 12864 of french CNRS, the *Dirección General de Investigación (MCyT)* and FEDER through the project TIC2001-1754 and the Consejería de Educación y Cultura de la Junta de Castilla y León through the project SA057/02.

References

[1] Terahertz Sources and Systems. Ed. by R.E. Miles, P. Harrison and D. Lippens. NATO Science Series: II. Mathematics, Physics and Chemistry – vol. 27 (Kluwer Academic Publishers, Dordrecht, 2001) 349 p.
[2] M. Urban, Ch. Nieswand, M. R. Siegrist, and F. Keilmann, J. Appl. Phys. **77**, 981 (1995).
[3] R. Brazis, R. Ragoutis, and M. R. Siegrist, J. Appl. Phys. **84**, 3474 (1998).
[4] D. Persano Adorno, M. Zarcone, and G. Ferrante, Laser Physics **10**, 310 (2000).
[5] R. Brazis, R. Raguotis, Ph. Moreau, and M. R. Siegrist, Int. J. Infrared and Millimeter Waves **21**, 593 (2001).
[6] D. Persano Adorno, M. Zarcone, and G. Ferrante, Laser Physics **11**, 291 (2001).
[7] P. Shiktorov, E. Starikov, V. Gružinskis, M. Zarcone, D. Persano Adorno, G. Ferrante, L. Reggiani, L. Varani, and J. C. Vaissière, phys. stat. sol. (a) **190**, 271 (2002).
[8] P. Shiktorov, E. Starikov, V. Gružinskis, L. Reggiani, L. Varani, J. C. Vaissière, T. González, and S. Pérez, IEEE Trans. Electr. Dev. **30**, 1171 (2003).
[9] T. W. Crowe, Int. J. Infrared Millim. Waves **10**, 765 (1989).
[10] A. Jelenski, A. Grub, V. Krozer, and H. L. Hartnagel, IEEE Trans. Microwave Theory Techn. **41**, 549 (1993).
[11] B. L. Gelmont, D. L. Woolard, J. L. Hesler, and T. W. Crowe, IEEE Trans. Electr. Dev. **45**, 2521 (1998).
[12] T. W. Crowe, J. L. Hesler, R. W. Weikle, and S. H. Jones, Infrared Phys. Technol. **40**, 175 (1999).
[13] W. Fawcett, A. D. Boardman, and S. Swain, J. Phys. Chem. Solids **31**, 1963 (1970).
[14] K. Brennan and K. Hess, Solid-State Electron. **27**, 347 (1984).
[15] B. E. Foutz, S. K. O'Leary, M. S. Shur, and L. F. Eastman, J. Appl. Phys. **85**, 7727 (1999).
[16] M. V. Fischetti and S. E. Laux, Phys. Rev. B **38**, 9721 (1988).
[17] V. Mitin, V. Gružinskis, E. Starikov, and P. Shiktorov, J. Appl. Phys. **75**, 935 (1994).
[18] T. Gonzalez, D. Pardo, L. Reggiani, and L. Varani, J. Appl. Phys. **82**, 2349 (1997).
[19] L. Varani, J. C. Vaissiere, J. P. Nougier, P. Houlet, L. Reggiani, E. Starikov, P. Shiktorov, V. Gružinskis, and L. Hlou, J. Appl. Phys. **77**, 665 (1995).